

Using the Aerasense NanoTracer for simultaneously obtaining several ultrafine particle exposure metrics

J Marra¹

Philips Research Laboratories, HTC 4, 5656 AE Eindhoven, The Netherlands

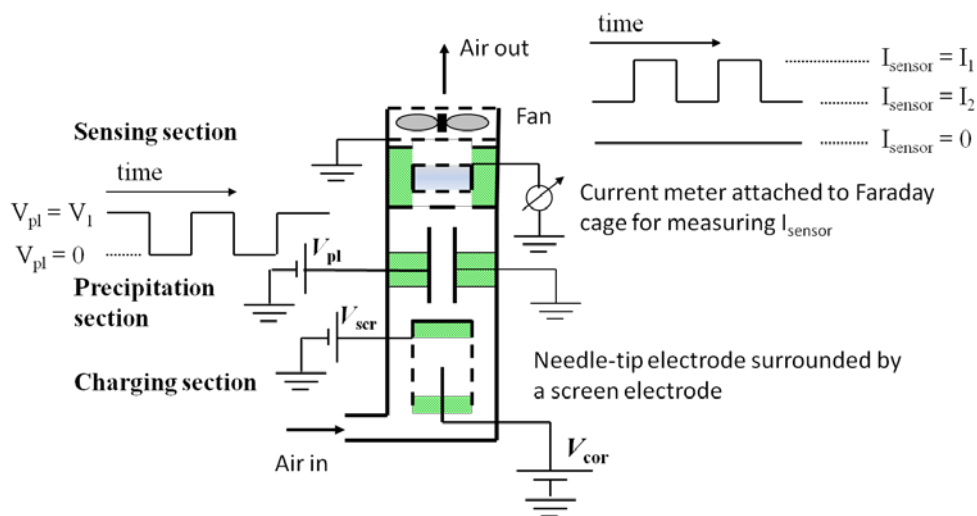
E-mail: johan.marra@philips.com

Abstract. The expanding production and use of nanomaterials increases the chance of human exposure to engineered nanoparticles (NP), also referred to as ultrafine particles (UFP; $\leq 100 - 300$ nm). This is particularly true in workplaces where they can become airborne and thereafter inhaled by workers during nanopowder processing. Considering the suspected hazard of many engineered UFPs, the general recommendation is to take measures for minimizing personal exposure while monitoring the UFP pollution for assessment and control purposes. The portable Aerasense NanoTracer accomplishes this UFP monitoring, either intermittently or in real time. This paper reviews its design and operational characteristics and elaborates on a number of application extensions and constraints. The NanoTracer's output signals enable several UFP exposure metrics to be simultaneously inferred. These include the airborne UFP number concentration and the number-averaged particle size, serving as characteristics of the pertaining UFP pollution. When non-hygroscopic particles are involved, the NanoTracer's output signals also allow an estimation of the lung-deposited UFP surface area concentration and the lung-deposited UFP mass concentration. It is thereby possible to distinguish between UFP depositions in the alveolar region, the trachea-bronchial region and the head airway region, respectively, by making use of the ICRP particle deposition model.

1. Introduction

Ultrafine particles (UFPs) are widely used for manufacturing nanostructured materials and for improving certain characteristics of more conventional materials. In recent years, stakeholders in the nanotech industry have expressed concern about the safety aspects associated with the use of engineered UFPs [1]. They can become airborne during their manufacture or handling and may subsequently find their way into the body through inhalation or skin contact. Evidence exists that after UFP inhalation, they may enter from the lung into the blood stream, thereby allowing them to reach, penetrate and subsequently damage the cells of vital organs [2-5]. Toxicological studies indicated that, per unit particle mass, exposure to particles becomes relatively more hazardous at decreasing particle size [6]. This applies in particular to water-insoluble solid particles and for particles comprising hazardous or reactive adsorbates on their surface. It has therefore been proposed to involve a particle surface area concentration metric in case the severity of the UFP air pollution is to be assessed, thereby accounting for all particles up to a size limit which is at least 100 nm but possibly as high as 300 nm [6-8]. This may be done in addition to the more commonly used PM₁₀ particle mass concentra-

Figure 1.
The Aerasense
NanoTracer.



tion metric for assessing ambient air pollution with respirable fine particles ($d_p \leq 10 \mu\text{m}$).

The intrinsic toxicity of engineered UFPs for humans is often difficult to assess and this complicates the setting of specific safety standards and regulations that involve one or more UFP concentration metrics [9-10]. The currently recommended safety policy is therefore a precautionary one aiming at exposure minimization in general and advocating in-situ control by monitoring both the workplace pollution level and the personal exposure to UFPs. This implies a need for robust and reliable UFP monitors that lend themselves for routine use by workers in the nano-industry. Preferably, they are portable and battery-powered while being able to relay relevant metrics in real time about the pertaining UFP pollution level. The Aerasense NanoTracer meets these demands and was described and benchmarked before in [11]. Ref. [12] discusses several of its applications. The present paper extends on [11] and presents additional features and conceptual constraints of the NanoTracer. To put them into perspective, a brief introduction about the NanoTracer is given first.

2. The NanoTracer's design and operation characteristics

Figure 1 shows the schematic design of the NanoTracer. It comprises a ventilator drawing a controlled airflow ϕ through the monitor. Particles in this airflow first enter the charging section, which comprises a porous screen electrode, set at V_{scr} , surrounding a high-voltage needle electrode that is set at a sufficiently high voltage V_{cor} to emit a constant corona current I_{cor} over time. The transmitted fraction of I_{cor} through the screen electrode induces diffusion charging of airborne particles through ion attachment. Charged particles subsequently enter the precipitation section wherein they are subjected to a block-shaped electric field pulse between two electrodes varying between $E_{pl} = V_1/d_{pl}$ and $E_{pl} = 0$. The electrodes have a travelling length L_{pl} and spacing d_{pl} . V_1 is chosen such that only a partial precipitation of charged particles with $d_p = 10 - 15 \text{ nm}$ is obtained. This implies that all larger particles will also only partially precipitate. The airflow carries all non-precipitated particles from the precipitation section into the sensing section where a fibrous filter captures them with their charge inside a Faraday cage. A sensitive current meter connects the Faraday cage to a reference potential and records the currents I_1 and I_2 that correspond with the application of $E_{pl} = 0$ and $E_{pl} = V_1/d_{pl}$, respectively, in the precipitation section. I_1 and I_2 are the sensor signals and equal the captured particle charge per unit time.

The difference $I_1 - I_2$ accounts for the precipitated amount of particle charge per unit time inside the precipitation section and is represented by

$$I_1 - I_2 = \int_{dp=0}^{\infty} \sum_{q=0}^{\infty} qe\phi_f(N_{ion}t_r, d_p) \xi_q(d_p, E_{pl}) d(N(d_p)) \quad (1)$$

$\xi_q(d_p, E_{pl})$ is the precipitated fraction of particles with diameter d_p carrying “q” elementary charges according to

$$\xi_q(d_p, E_{pl}) = 1 \quad \text{when} \quad \frac{qeC_c(d_p)E_{pl}L_{pl}}{3\pi\eta_{air}d_p v_{air}d_{pl}} \geq 1 \quad (\text{full precipitation})$$

$$\xi_q(d_p, E_{pl}) = \frac{qeC_c(d_p)E_{pl}L_{pl}}{3\pi\eta_{air}d_p v_{air}d_{pl}} \quad \text{otherwise} \quad (2)$$

v_{air} is the average airspeed between the electrodes in the precipitation section, $N(d_p)$ the number concentration of particles with diameter d_p , η_{air} the viscosity of air, and “e” the elementary charge. $N_{ion}t_r$ denotes the product of the average ion concentration in the charging section and the particle residence time therein. $f_q(N_{ion}t_r, d_p)$ is the fraction of all particles of diameter d_p charged with “q” elementary charges and relates to the average particle charge $Q(d_p)$ according to

$$Q(d_p) = \sum_{q=0}^{\infty} qf_q(N_{ion}t_r, d_p) \quad (3)$$

Numerical values for $f_q(N_{ion}t_r, d_p)$ are predicted by the Fuchs theory for particle diffusion charging [13].

When $E_{pl} = 0$, the signal I_1 is obtained which represents the total airborne particle charge as

$$I_1 = \int_{dp=0}^{\infty} \sum_{q=0}^{\infty} qe\phi_f(N_{ion}t_r, d_p) d(N(d_p)) \quad (4)$$

The NanoTracer’s design and process parameters in combination with the measured ion current transmitted through the screen electrode were found to be consistent with a numerical value for the charging parameter $N_{ion}t_r = 0.5 - 0.7 \times 10^{13}$ ions.m⁻³.s. According to the Fuchs theory, the latter value implies a substantially linear dependence of $Q(d_p)$ on d_p . This was experimentally confirmed [11].

3. UFP pollution and exposure assessment with the NanoTracer

For characterizing the UFP pollution level, it is desirable to have knowledge about the total UFP number concentration N and the size distribution $N(d_p)$. For exposure assessment, both the deposited UFP surface area concentration and the deposited UFP mass concentration can be relevant metrics.

3.1 Obtaining the UFP number concentration N and average particle size $d_{p,av}$

The proportionality $Q(d_p) \propto d_p$ leads to a direct proportionality between I_1 and the particle length

concentration $L = \int_{dp=0}^{\infty} d_p d(N(d_p)) = Nd_{p,av}$, with $d_{p,av}$ the number-averaged particle size, because

$$I_1 = \int_{dp=0}^{\infty} \sum_{q=0}^{\infty} qe\phi_f(N_{ion}t_r, d_p) dN(d_p) \propto \int_{dp=0}^{\infty} \sum_{q=0}^{\infty} qf_q(N_{ion}t_r, d_p) dN(d_p)$$

$$\propto \int_{dp=0}^{\infty} Q(d_p) dN(d_p) \propto \int_{dp=0}^{\infty} d_p dN(d_p) = Nd_{p,av} \quad (5)$$

Another consequence (see ref. [11]) is that both N and $d_{p,av}$ can be inferred from I_1 and I_2 according to

$$N = S_N (I_1 - I_2) \quad (6)$$

$$d_{p,av} = S_{dp} \frac{I_1}{I_1 - I_2} \quad (7)$$

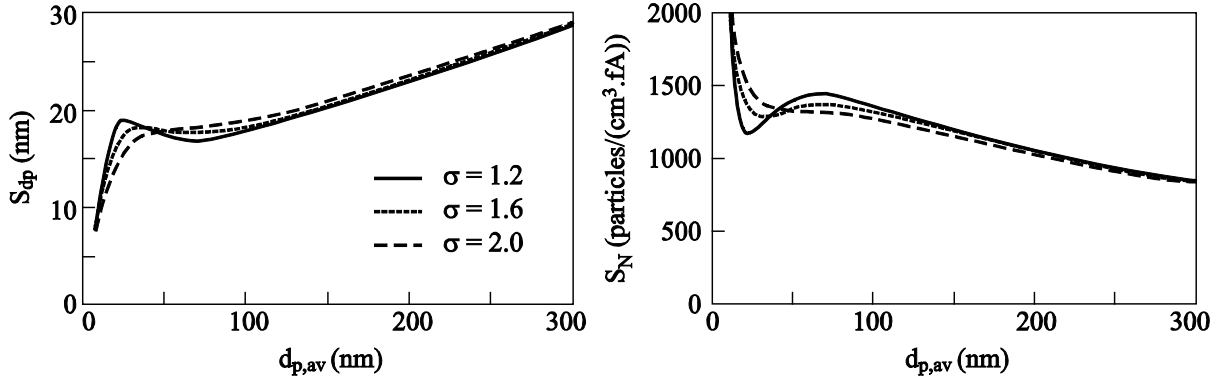


Figure 2. S_{dp} and S_N values according to the ICRP model for a mono-modal log-normal particle size distribution at $N_{ion,lr} = 0.6 \times 10^{13}$ ions. m^{-3} .s and $\phi = 0.45$ liter/min, as existing in the NanoTracer.

within the average particle size domain wherein the proportionality constants S_N and S_{dp} are substantially independent of $d_{p,av}$ and the particle size distribution characteristics. It was shown in [11] that this size domain exists in the $20 \text{ nm} \leq d_{p,av} \leq 100 \text{ nm}$ region which includes particles with $d_p > 100 \text{ nm}$. Knowledge of $d_{p,av}$ gives some insight in the UFP size distribution and, as will be shown below, is often sufficient for deriving appropriate UFP exposure metrics.

It is of interest to investigate the validity of equations (6) and (7) when $d_{p,av} > 100 \text{ nm}$. This was done by substituting equations (1) and (4) into (6) and (7) at a given N as a function of $d_{p,av}$ and σ . σ is the standard deviation of the used log-normal particle size distribution $N(d_p)$ according to

$$dN(d_p) = \frac{N}{\sqrt{2\pi} \ln \sigma} \exp \left[-\frac{(\ln d_p - \ln d_{p,av} + 0.5 \ln^2 \sigma)^2}{2(\ln \sigma)^2} \right] d \ln(d_p) \quad (8)$$

Results are shown in Figure 2 for $d_{p,av} \leq 300 \text{ nm}$ at the existing ratio $\frac{E_{pl} L_{pl}}{v_{air} d_{pl}} = 1.927 \times 10^6 \text{ V.s/m}^2$

inside the NanoTracer. They reveal that σ only marginally affects S_N and S_{dp} . At a commonly encountered value $\sigma = 1.6$, the outcome for S_N and S_{dp} in equations (6) and (7) is that

$$S_{dp} = S_{dp}^* \quad S_N = S_N^* \quad 20 \text{ nm} \leq d_{p,av} \leq 100 \text{ nm} \quad (9)$$

$$S_{dp} \approx S_{dp}^* (0.714 + 2.86 \times 10^{-3} d_{p,av}) \quad S_N \approx \frac{S_N^*}{0.714 + 2.86 \times 10^{-3} d_{p,av}} \quad d_{p,av} \geq 100 \text{ nm} \quad (10)$$

At $\frac{E_{pl} L_{pl}}{v_{air} d_{pl}} = 1.927 \times 10^6 \text{ V.s/m}^2$, one has $S_{dp}^* = 18 \text{ nm}$ and $S_N^* = 1340 \text{ particles.cm}^{-3}.\text{fA}^{-1}$, almost

independent of $d_{p,av}$. For $d_{p,av} > 100 \text{ nm}$, the combination of equations (6), (7), (9) and (10) results in

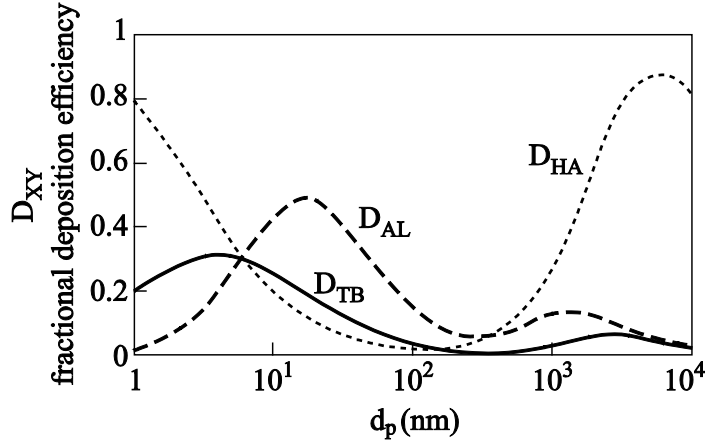
$$d_{p,av} = \frac{0.714 S_{dp}^* I_1}{(I_1 - I_2) - 2.86 \times 10^{-3} S_{dp}^* I_1} \quad N = \frac{S_N^* (I_1 - I_2)}{0.714 + 2.86 \times 10^{-3} d_{p,av}} \quad (11)$$

I_1 and I_2 in (11) and (12) must be expressed in ‘fA’, yielding N in ‘particles/cm³’ and $d_{p,av}$ in ‘nm’.

3.2. Obtaining the lung-deposited UFP surface area and mass concentrations

As mentioned above, evidence exists that when solid water-insoluble particles are involved, much of the health risk associated with UFP inhalation is probably associated with the actually deposited UFP surface area concentration in the lung. UFP deposition in the deep alveolar (AL) region of the lung

Figure 3. Fractional particle depositions D_{AL} , D_{TB} and D_{HA} of inhaled (spherical) particles in the AL, TB and HA regions of the respiratory tract, respectively, according to the ICRP model for a reference person.



where gas exchange with the blood occurs is particularly relevant, because they can persist there for extended periods and even find their way into the blood stream. UFP deposition in the head airways (HA) is not *a priori* harmless either, because of possible UFP transport from the nose via the olfactory nerve into the brain [5].

On the other hand, the deposited mass concentration remains a relevant exposure metric for water-soluble or liquid-phase UFPs. Many toxicologists still prefer the use of the mass concentration metric for any type of particle in combination with the average particle size. Hence, it would be convenient to be able to infer both the UFP surface area concentration and the UFP mass concentration that deposit in the lung from inhaled air. This might sometimes deal with the problem that the NanoTracer itself cannot recognise the chemical composition, shape and phase state of airborne particles.

The ICRP model (International Commission on Radiological Protection, Publication 66, 1994) for a reference person describes the fractional deposition of inhaled non-hygroscopic spherical particles in the head airway (HA) region, the trachea-bronchial (TB) region and the alveolar (AL) region of the respiratory tract. Analytical equations for the corresponding deposited fractions $D_{HA}(d_p)$, $D_{TB}(d_p)$ and $D_{AL}(d_p)$ are available from the literature [14] and depicted in Figure 3. They can be used to derive the deposited surface area concentrations S_{XY} ($XY = HA, TB$ or AL) as

$$S_{XY}(d_{p,max}) = \int_{dp=0}^{dp,max} \pi d_p^2 D_{XY}(d_p) dN(d_p) \quad (13)$$

for particles in the $0 \leq d_p \leq d_{p,max}$ size region. The deposited mass concentration M_{XY} is given by

$$M_{XY}(d_{p,max}) = \int_{dp=0}^{dp,max} \rho_p \frac{\pi d_p^3}{6} D_{XY}(d_p) dN(d_p) \quad (14)$$

ρ_p is the particle density. Figure 4 present calculated results for $S_{XY}(d_{p,max})$ as a function of $d_{p,av}$ in the AL and TB lung compartments, respectively, for $d_{p,max} \rightarrow \infty$ and several mono-modal log-normal particle size distributions according to equation (13). Within the size interval $20 \text{ nm} \leq d_{p,av} \leq 100 \text{ nm}$, they can be estimated with the linear equations (see Figure 4)

$$S_{AL} = 4.7 \times 10^{-5} N d_{p,av} = 4.7 \times 10^{-5} S_N^* S_{dp}^* I_1 \quad (15)$$

$$S_{TB} = 0.95 \times 10^{-5} N d_{p,av} = 0.95 \times 10^{-5} S_N^* S_{dp}^* I_1 \quad (16)$$

Results for S_{HA} are given in Figure 5 for $d_{p,max} \rightarrow \infty$ and $d_{p,max} = 200 \text{ nm}$. It is evident that when only the deposition of UFPs is concerned up to $d_p = 200 \text{ nm}$, the deposition results in the HA region can also be estimated with a linear equation according to

$$S_{HA} = 0.6 \times 10^{-5} N d_{p,av} = 0.6 \times 10^{-5} S_N^* S_{dp}^* I_1 \quad (17)$$

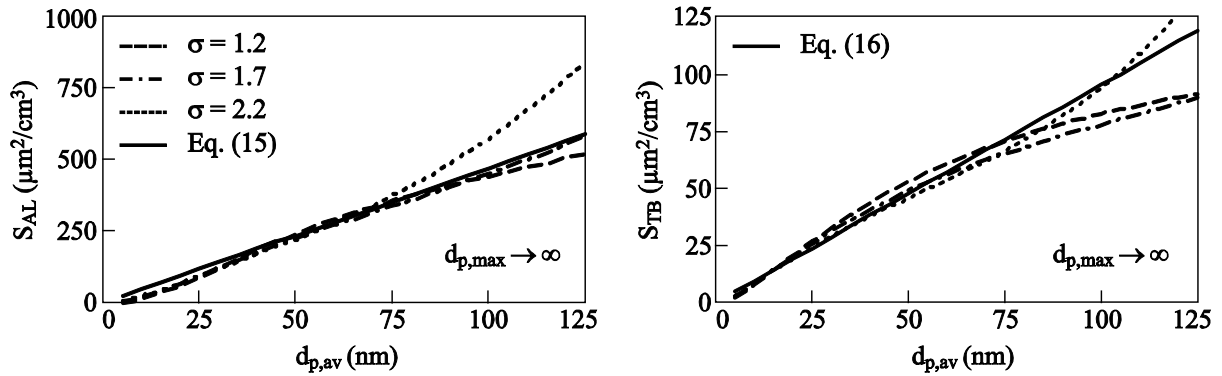


Figure 4. Surface area concentrations S_{XY} that deposit in the AL and TB lung regions, respectively, at $N = 10^5$ particles/cm³ and $d_{p,max} \rightarrow \infty$ according to the ICRP model.

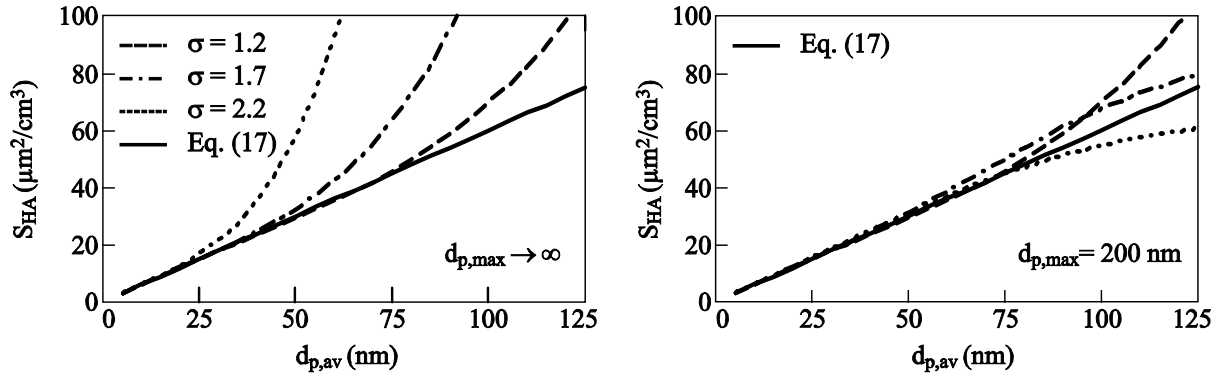


Figure 5. S_{HA} at $N = 10^5$ particles/cm³ for $d_{p,max} \rightarrow \infty$ and $d_{p,max} = 200$ nm, respectively.

In equations (15) – (17), S_{XY} is obtained in “ $\mu\text{m}^2/\text{cm}^3$ ” when I_1 is substituted in “fA”, S_{dp}^* in “nm”, S_N^* in “particles/(cm³.fA)”, N in “particles/cm³” and $d_{p,av}$ in “nm”. Deposited surface area concentrations are therefore in all cases approximately proportional to the output signal I_1 . The numerical values of and ratios between the various S_{XY} values are comparable to those obtained in [15] with the Nanoparticle Surface Area Monitor (NSAM, TSI model 3550). One difference is that the S_{XY} results obtained for the NanoTracer are explicitly obtained in terms of N and $d_{p,av}$ whereas separate values for N and $d_{p,av}$ cannot be obtained with the NSAM. The NSAM operates according to a different particle charging and precipitation strategy.

Examples of calculated values $M_{XY}(d_{p,max})$ are presented in Figures 6 - 8. Here, σ plays a prominent role when $\sigma > 1.7$ at $d_{p,max} \rightarrow \infty$, particularly concerning the results for $M_{HA}(d_{p,max})$. This is due to the sharp upswing in $D_{HA}(d_p)$ at $d_p > 300$ nm (see Figure 3). Less influence from σ exists when $d_{p,max}$ is limited to 250 nm for $d_{p,av} \leq 75$ nm in the AL and TB regions. The solid lines in Figures 6 - 8 obey the relationships:

for $d_{p,max} \rightarrow \infty$:

$$M_{AL} = N\rho_p \times 10^{-5} \left[-3.28 \times 10^{-7} d_{p,av}^3 + 8.79 \times 10^{-4} d_{p,av}^2 + 1.08 \times 10^{-3} d_{p,av} \right] \quad (18)$$

at $\sigma \leq 1.7$; $d_{p,av} \leq 100$ nm

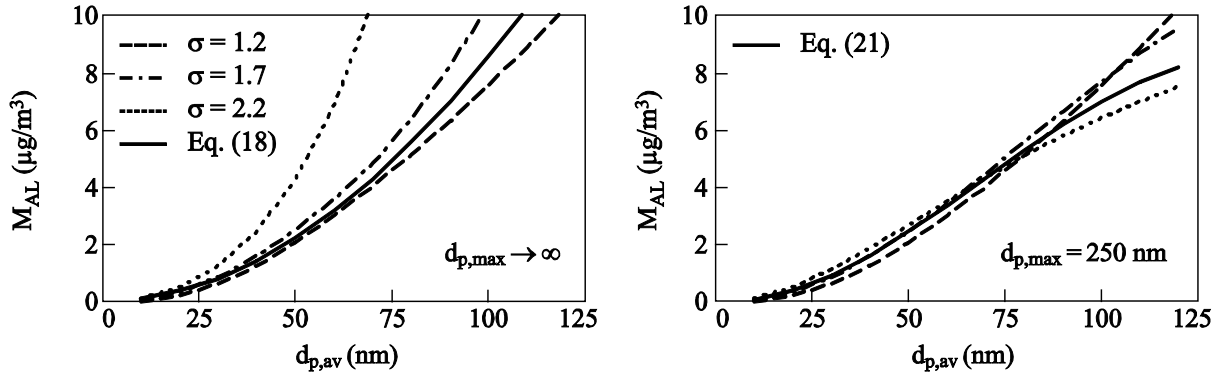


Figure 6. Deposited mass concentrations M_{AL} at $N = 10^5$ particles/ cm^3 and $\rho_p = 1$ gram/ cm^3 for $d_{p,max} \rightarrow \infty$ and $d_{p,max} = 250$ nm, respectively, according to the ICRP model.

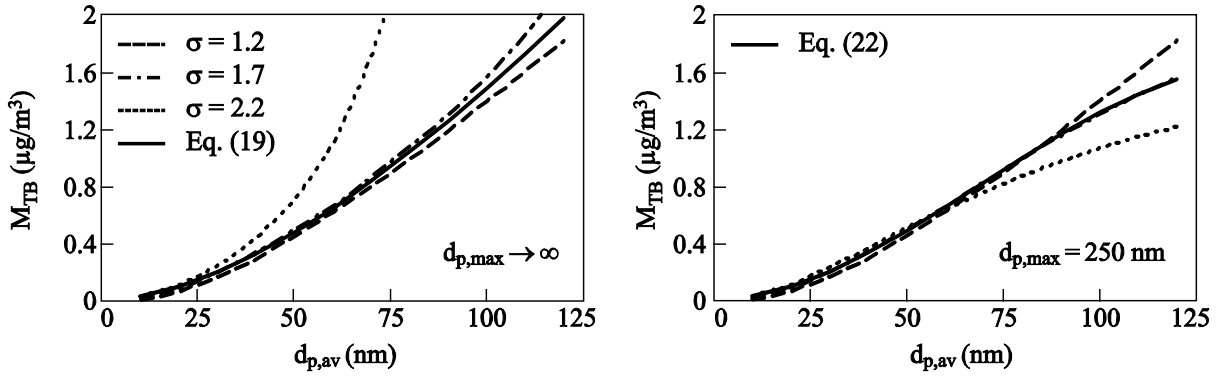


Figure 7. Deposited mass concentrations M_{TB} at $N = 10^5$ particles/ cm^3 and $\rho_p = 1$ gram/ cm^3 for $d_{p,max} \rightarrow \infty$ and $d_{p,max} = 250$ nm, respectively, according to the ICRP model.

$$M_{TB} = N\rho_p \times 10^{-5} \left[-4.415 \times 10^{-7} d_{p,av}^3 + 1.74 \times 10^{-4} d_{p,av}^2 + 1.916 \times 10^{-3} d_{p,av} \right] \quad (19)$$

at $\sigma \leq 1.7$; $d_{p,av} \leq 120$ nm

$$M_{HA} = N\rho_p \times 10^{-5} \left[9.05 \times 10^{-7} d_{p,av}^3 - 2.63 \times 10^{-6} d_{p,av}^2 + 2.538 \times 10^{-3} d_{p,av} \right] \quad (20)$$

at $\sigma \leq 1.2$; $d_{p,av} \leq 120$ nm

for $d_{p,max} = 250$ nm:

$$M_{AL} = N\rho_p \times 10^{-5} \left[-7.516 \times 10^{-6} d_{p,av}^3 + 1.547 \times 10^{-3} d_{p,av}^2 - 9.42 \times 10^{-3} d_{p,av} \right] \quad (21)$$

at $\sigma \leq 2.2$; $d_{p,av} \leq 100$ nm

$$M_{TB} = N\rho_p \times 10^{-5} \left[-1.144 \times 10^{-6} d_{p,av}^3 + 2.39 \times 10^{-4} d_{p,av}^2 + 7.107 \times 10^{-4} d_{p,av} \right] \quad (22)$$

at $\sigma \leq 2.2$; $d_{p,av} \leq 80$ nm

$$M_{HA} = N\rho_p \times 10^{-5} \left[9.05 \times 10^{-7} d_{p,av}^3 - 2.63 \times 10^{-6} d_{p,av}^2 + 2.538 \times 10^{-3} d_{p,av} \right] \quad (23)$$

at $\sigma \leq 1.2$; $d_{p,av} \leq 120$ nm

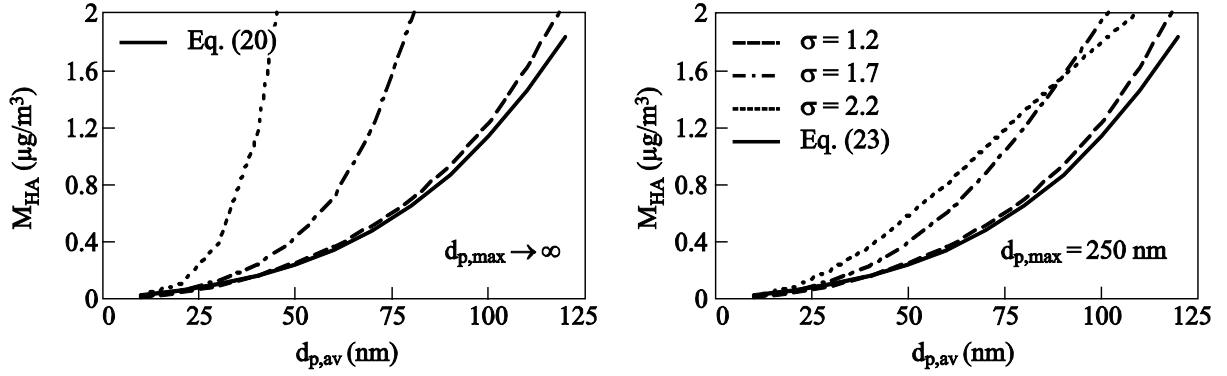


Figure 8. Deposited mass concentrations M_{HA} at $N = 10^5$ particles/cm³ and $\rho_p = 1$ gram/cm³ for $d_{p,\text{max}} \rightarrow \infty$ and $d_{p,\text{max}} = 250$ nm, respectively, according to the ICRP model.

In equations (18) – (23), $d_{p,\text{av}}$ must be expressed in “nm”, N in “particles/cm³” and ρ_p in “gram/cm³”, yielding M_{XY} in “μg/m³”. Equations (18) – (23) show that when certain conditions are met w.r.t. σ and $d_{p,\text{av}}$, it is possible to deduct estimates for M_{XY} from the inferred values for N and $d_{p,\text{av}}$ obtained from I_1 and I_2 according to equations (6) – (12). More precise predictions are obtained when the particle size distribution is known upfront. It must be noted though that the accuracy of any calculated exposure metric is inherently limited due to person-to-person variability in the functions $D_{\text{XY}}(d_p)$ shown in Figure 3.

4. The NanoTracer’s sensitivity towards UFP and FP mass concentration changes

Other than for UFP monitoring in workplaces, the NanoTracer can also be used for more general environmental air pollution monitoring. Particle pollution in outdoor air is traditionally quantified in terms of the particle mass concentration PM_{10} of all airborne fine particles (FP) with $d_p \leq 10$ μm, which can potentially reach and deposit in the alveolar region (see Figure 3). These include UFPs with $10 \text{ nm} \leq d_p \leq 300 \text{ nm}$, but their mass is normally small in comparison with the mass of FPs with $300 \text{ nm} \leq d_p \leq 10 \text{ μm}$. It was argued before that the UFP mass concentration metric for inhaled solid UFPs is not likely to be the most suitable exposure metric for quantifying their exposure risk. It would therefore make sense to distinguish UFPs from FPs as two distinct classes of respirable particles, each being assessed with a different metric.

It is instructive to investigate the relative sensitivity of the NanoTracer signals to changes in the airborne particle mass concentration M at various values of $d_{p,\text{av}}$ in order to assess the NanoTracer’s application constraints. M is obtained from

$$M = \int_{d_p=0}^{\infty} \rho_p \frac{\pi d_p^3}{6} dN(d_p) \quad (24)$$

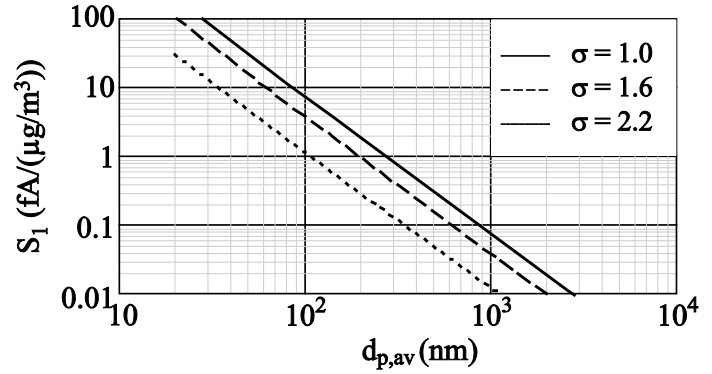
A sensitivity number $S_1(d_{p,\text{av}}, \sigma)$ can be defined according to

$$S_1(d_{p,\text{av}}, \sigma) = \left(\frac{d(I_1)}{dM} \right)_{d_{p,\text{av}}, \sigma} \times 10^6 = \left(\frac{d(I_1)}{dN} \cdot \frac{dN}{dM} \right)_{d_{p,\text{av}}, \sigma} \times 10^6 = \frac{I_1}{M} \times 10^6 \quad (25)$$

wherein a constant log-normal particle size distribution is assumed to exist (i.e. constant values for $d_{p,\text{av}}$ and σ) and wherein changes in M are therefore only due to changes in N . For monodisperse particles ($\sigma = 1$), the explicit result is

$$S_1(d_{p,\text{av}}, \sigma) = S_1(d_p, 1) = \frac{6Q(d_p)e\phi}{\rho_p \pi d_p^3} \times 10^6 \quad (26)$$

Figure 9. The NanoTracer sensitivity number S_1 as a function of $d_{p,av}$ and σ .



wherein all parameters must be substituted in SI units, yielding $S_1(d_{p,av}, \sigma)$ in “fA/($\mu\text{g}\cdot\text{m}^{-3}$)”. The NanoTracer’s specifications include $N_{\text{ion}t_r} \approx 0.6 \times 10^{13}$ ions.s.m⁻³ and $\phi = 0.45$ liter/min, leading to

$$Q(d_p) = 0.0326 \times 10^9 d_p \quad (27)$$

(d_p in “m”).

The fine particle PM_{10} concentration in moderately polluted air is about $10 \mu\text{g}/\text{m}^3$ and may increase to over $100 \mu\text{g}/\text{m}^3$ in seriously polluted air. It appears reasonable therefore to evaluate $S_1(d_{p,av}, \sigma)$ as the measured change ΔI_1 when $\Delta M = 1 \mu\text{g}/\text{m}^3$. Results for monodisperse and two heterodisperse particle distributions are shown in Figure 9. Figure 9 shows a markedly decreasing $S_1(d_{p,av}, \sigma)$ at increasing $d_{p,av}$ and σ . A satisfactory measuring sensitivity towards FPs ($d_p > 300$ nm) exists when $S_1(d_p, 1) \geq 1 \text{ fA}/(\mu\text{g}\cdot\text{m}^{-3})$, also in view of the NanoTracer’s noise level $\Delta I_1 = \pm 1$ fA. Figure 9 indicates that the NanoTracer falls short of this demand at $d_{p,av} > 300$ nm, thereby highlighting the NanoTracer’s primary function as a UFP monitor for particles with $d_{p,av} \leq 300$ nm. Note that $S_1(d_{p,av}, \sigma) \propto \phi$. $S_1(d_{p,av}, \sigma)$ can therefore in theory be increased up to any desired level by increasing ϕ albeit at the expense of a proportional increase in the equipment size. But I_1 will always remain more sensitive to UFP mass concentration changes than to FP mass concentration changes.

5. Application constraints of the NanoTracer

The presented equations for the deduction of N , $d_{p,av}$, S_{XY} and M_{XY} hold for single particles with a more-or-less spherical shape whose charging behavior follows the predictions of the Fuchs theory [13]. Several application examples are described in [12] concerning (N , $d_{p,av}$) measurements in the HVAC unit of an office building, in a workplace, a home, a driving automobile and outdoors. However, shape and composition of the measured particles remain unknown and the existence of a spherical particle shape is not guaranteed. Part of the UFPs and FPs in workplaces may be encountered as loosely structured aggregates composed of many primary particles [16]. The size distribution of aggregate mobility diameters d_m can be readily inferred with a SMPS but d_m cannot simply replace the geometric diameter d_p used by the Fuchs theory. The aggregate’s charging behavior also depends on its fractal dimension and the primary particle size d_{prim} [16-17]. These are usually not known upfront. Interpreting sensor signals in the presence of mixtures of single particles and particle aggregates is therefore also problematic, although this depends on the desired accuracy. Within a restricted size range for $d_{p,av}$, the relationship between I_1 and N is foreseen [16] to have the general form

$$N = \frac{C}{d_{p,av}^a} I_1 \quad (28)$$

“a” and “C” are parameters that depend on d_{prim} and the fractal particle dimension. For single spherical particles, $a = 1.0$ and $C = S_N^* S_{dp}^*$. The proportionality $N \propto I_1$ holds at constant $d_{p,av}$, σ , and d_{prim} .

An informative example in this regard is given in Figure 10 where preliminary NanoTracer measurements on airborne fractal carbon aggregates are shown as a function of N and $d_{p,av}$. The carbon aggregates were produced by a Combustion Aerosol STAndards generator (CAST) manufactured by

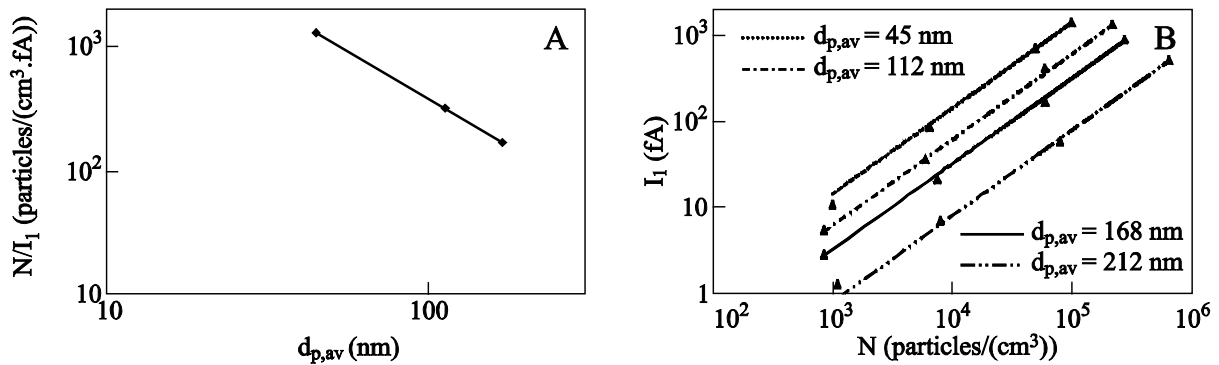


Figure 10. Measured ratio N/I_1 and signal I_1 for carbon aggregates produced by the CAST generator.

Jing Ltd., Switzerland. Data for N , σ and $d_{p,av}$ were obtained with a SMPS (Model 3936, TSI Inc.) and compared with the NanoTracer's I_1 data. The aggregates had a log-normal size distribution with $\sigma \approx 1.6$. At each average aggregate mobility diameter $d_{p,av}$, Figure 10B shows that the relationship $N \propto I_1$ indeed holds. The slope of the curve in Figure 10A is consistent with $a = 1.5$, thus equations (6) and (7) no longer apply. It is unknown to which extent possible changes in d_{prim} may have affected the slope of the curve in Figure 10A when changing $d_{p,av}$. The CAST product literature shows that the produced carbon aggregates have a pronounced fractal character, more so than that of typical soot aggregates encountered in diesel exhaust. The deviation of the parameter values “C” and “a” in equation (28) from the corresponding values predicted by the Fuchs theory for spherical particles are therefore likely to be larger for the CAST aggregates than for diesel soot aggregates, though this awaits experimental confirmation. Apart from that, the deduction of reasonably accurate (N , $d_{p,av}$) data with equations (6) and (7) is expected to remain possible when dealing with a defined source of particles (e.g. diesel exhaust) that emit aerosols of a more-or-less reproducible composition, size distribution and aggregate characteristics. The source-specific parameters S_N^* , S_{dp}^* can then be ad-hoc determined through calibration with other aerosol instruments, notably the CPC and/or the SMPS.

Another issue concerns the particle hygroscopicity. Inferred numbers for S_{XY} and M_{XY} in the presence of spherical particles can be relied upon only when non-hygroscopic particles are involved. Hygroscopic particles substantially increase in size when entering the high-humidity environment of the respiratory tract, which drastically changes their deposition behavior [18 – 19]. When inhaled particles do not comprise water-soluble (ionic) species, substantial hygroscopic growth inside the lung will not occur. This is true for many engineered UFPs.

The particle size d_p in Figure 3 refers to the aerodynamic particle diameter. For single particles, the aerodynamic diameter equals the electrical mobility diameter and, for particles with $d_p < 200$ nm, also equals the geometric particle diameter irrespective of ρ_p [15]. It is therefore usually justified to neglect the influence of ρ_p on S_{xy} . On the other hand, M_{xy} always remains proportional to ρ_p .

6. Conclusion

The Aerasense NanoTracer is a portable electrical UFP monitor device designed to serially generate two independent electrical signals I_1 and I_2 from diffusion-charged airborne particles. Under the assumption that the extent of particle charging reasonably agrees with the predictions of the Fuchs theory, these signals can be used to determine the N and $d_{p,av}$ of airborne particles in the $10 \text{ nm} < d_p < 500 \text{ nm}$ size region, thereby partly characterizing the existing airborne UFP pollution. Larger FPs are also measured but their contribution to the generated signals is usually only small. The interpretation of I_1 and I_2 in terms of N and $d_{p,av}$ becomes less accurate when the UFP pollution is substantially comprised of particles with a pronounced fractal aggregate structure. No evidence exists that this

occurs in typical ambient or workplace environments but it can be relevant when the particle emission from specific sources must be characterized. When such sources emit aggregates with a reasonably constant size distribution and composition, reliable characterization with a NanoTracer remains possible after ad-hoc calibration with a CPC and/or SMPS. Use of a NanoTracer has specific advantages because of its easy use, portability, small size and weight, its capability of almost real-time measuring, and the absence of a radioactive source and consumable liquids.

When solid non-hygroscopic water-insoluble particles are present, as is the case with most engineered UFPs, the measurement of only I_1 is sufficient for estimating the deposited UFP surface area concentrations S_{XY} from inhaled air in the various lung compartments. This follows from the ICRP deposition model. S_{XY} is a relevant exposure metric considering that the toxicity of deposited UFPs per unit particle mass increases when their surface area concentration increases.

The deposited UFP mass concentrations M_{XY} in the various lung compartments can simultaneously be estimated from the separately determined values for N and $d_{p,av}$. Reasonable estimates for M_{HA} are only possible when the UFP size distribution parameter σ is known upfront. The mass concentration metric is relevant when the deposited material is soluble and/or in the liquid state.

Complete risk assessment not only involves exposure assessment but also knowledge about the toxicity of the inhaled UFPs and the total inhaled amount of material over a certain period. Furthermore, when the (suspected) toxicity of the UFPs released in air at the workplace differs from that of the ambient UFPs produced by other sources (e.g. from outdoor air pollution), it is necessary to somehow distinguish between these two kinds of UFPs before an assessment of exposure and risk concerning the workplace-generated NPs can be carried out. An off-line chemical speciation of sampled UFPs remains necessary to assess the chemical characteristics of the polluting particles and can help to distinguish workplace-released engineered particles from ambient particles.

References

- [1] Balbus J M, Florini K, Denison R A and Walsh S A 2007 *J. Nanoparticle Res.* **9** 11
- [2] Kreyling W G, Semmler M, Erbe F, Mayer P, Takenaka S, Schultz H, Oberdörster G and Ziesenis A 2002 *J. Toxicol. Environ. Health* **A65** 1513
- [3] Oberdörster G 2000 *Philos. Trans. R. Soc. Lond.* **A358** 2719
- [4] Oberdörster G, Gelein R M, Ferin J and Weis B 1995 *Inhal. Toxicol.* **7** 111
- [5] Oberdörster E 2004 *Environ. Health Perspect.* **112** 1058
- [6] Oberdörster G, Oberdörster E and Oberdörster J 2005 *Environ. Health Perspect.* **113** 823
- [7] Donaldson K, Li X Y and MacNee W 1998 *J. Aerosol Sci.* **29** 553
- [8] Oberdörster G 1996 *Part. Sci. Technol.* **14** 135
- [9] Howard J and Murashov V 2009 *J. Nanoparticle Res.* **11** 1673
- [10] Murashov V, Engel S, Savolainen K, Fullam B, Lee M and Kearns P 2009 *J. Nanoparticle Res.* **11** 1587
- [11] Marra J, Voetz M and Kiesling H J 2010 *J. Nanoparticle Res.* **12** 21
- [12] Marra J, van den Brink W, Goossens H and Kessels S 2009 *IEEE Nanotech. Magazine* **3** (2) 6
- [13] Adachi M, Kousaka Y and Okuyama K 1985 *J. Aerosol Sci.* **16** 109
- [14] Hinds W C 1999 *Aerosol technology: properties, behaviour and measurement of airborne particles* Chapter 11, 2nd Ed. (New York: Wiley-Interscience)
- [15] Asbach C, Fissan H, Stahlmecke B, Kuhlbusch T A J and Pui D Y H 2009 *J. Nanoparticle Res.* **11** 101
- [16] Wang J, Shin W G, Mertler M, Sachweh B, Fissan H and Pui D Y H 2010 *Aerosol Science and Technology* **44** 97
- [17] Shin W G, Wang J, Mertler M, Sachweh B, Fissan H and Pui D Y H 2010 *J. Aerosol Sci.* **41** 975
- [18] Löndahl J, Massling A, Pagels J, Swietlicki E, Vaclavik E and Loft S 2007 *Inhal. Toxicol.* **19** 109
- [19] Asgharian B 2004 *Aerosol Science and Technology* **38** 938